



ELSEVIER

Contents lists available at ScienceDirect

Control Engineering Practice

journal homepage: www.elsevier.com/locate/conengprac

Design and evaluation of a unified chassis control system for rollover prevention and vehicle stability improvement on a virtual test track

Jangyeol Yoon^a, Wanki Cho^a, Juyong Kang^a, Bongyeong Koo^b, Kyongsu Yi^{a,*}

^a School of Mechanical and Aerospace Engineering, Seoul National University, 599 Gwanangno, Gwanak-Gu, Seoul 151-742, Republic of Korea

^b Mando Corporation Central R&D Center, 413-5 Gomae-Ri, Giheung-Eub, Yongin-Si, Kyonggi-Do 449-901, Republic of Korea

ARTICLE INFO

Article history:

Received 6 May 2009

Accepted 23 February 2010

Available online 23 March 2010

Keywords:

Full-scale driving simulator

Human-in-the-loop evaluation

Rollover mitigation control

Unified chassis control

Vehicle stability

Virtual test track

ABSTRACT

This paper describes the development of a unified chassis control (UCC) scheme and the evaluation of the control scheme on a virtual test track (VTT). The UCC scheme aims to prevent vehicle rollover, and to improve vehicle maneuverability and its lateral stability by integrating electronic stability control (ESC) and active front steering (AFS). The rollover prevention is achieved through speed control, and the vehicle stability is improved via yaw rate control. Since the UCC controller always works with the driver, the overall vehicle performance depends not only on how well the controller works but also on its interactions with the human driver. Vehicle behavior and the interactions between the vehicle, the controller, and the human driver are investigated through a full-scale driving simulator on the VTT which consists of a real-time vehicle simulator, a visual animation engine, a visual display, and suitable human–vehicle interfaces. The VTT has been developed and used for the evaluation of the UCC under various realistic conditions in the laboratory making it possible to evaluate the UCC controller in the laboratory without risk of injury prior to field testing, and promises to significantly reduce the cost of development as well as the overall cycle development time.

© 2010 Elsevier Ltd. All rights reserved.

1. Introduction

Vehicle rollover is a serious problem in the area of ground transportation and a report published by the National Highway Traffic Safety Administration (NHTSA) has found that, even though rollover constitutes only a small percentage of all accidents, it does, however constitute a disproportionately large portion of severe and fatal injuries. Almost 11 million passenger cars, SUVs, pickups, and vans crashed in 2002, yet only 2.6% of these involved a rollover. However, the percentage of fatal crashes that involved the occurrence of rollover was about 21.1%, which is significantly higher than the corresponding percentages for other types of crashes (NHTSA, 2003). In order to help consumers understand a vehicle's likelihood of rollover, the rollover resistance rating program was proposed by NHTSA which uses the static stability factor (SSF), which is the ratio of half the track width to the height of the center of gravity (CG), to determine the rollover resistance rating. The SSF has been questioned by the automotive industry as it does not consider the effects of suspension deflection, tire traction aspects, or the dynamics of the vehicle control system. Accordingly, in 2002, NHTSA

published another announcement with regard to a tentative dynamical rollover test procedure (NHTSA, 2001).

Most existing rollover prevention technologies can be classified into two types, namely, (1) the type which directly controls the vehicle roll motion through an active suspension, an active anti-roll bar, or an active stabilizer (Chen & Hsu, 2008) which can prevent rollover by raising the rollover threshold; and (2) the type which indirectly influences roll motions by controlling the yaw motions through differential braking and active front steering (Wielenga & Chace, 2000). Several studies have been undertaken on rollover detection and its prevention and Hac et al. have proposed an algorithm that detects impending rollover and an estimator-based roll index (Hac, Brown, & Martens, 2004). Chen and Peng proposed an anti-rollover algorithm based on the time-to-rollover (TTR) metric (Chen & Peng, 2001). In this research, differential braking is selected as the actuation methodology. Ungoren and Peng evaluated a vehicle dynamics control (VDC) system for rollover prevention (Ungoren & Peng, 2004). Yang and Liu proposed a robust active suspension for rollover prevention (Yang & Liu, 2003) and Schofield and Hagglund proposed a method for rollover prevention that employs an optimal tire force distribution (Schofield & Hagglund, 2008). Yoon and Yi proposed a rollover index that indicates the danger of vehicle rollover as well as an index-based rollover mitigation control system to reduce the rollover index through Electronic Stability Control (ESC) (Yoon, Kim, & Yi, 2007). Since the lateral acceleration is the

* Corresponding author. Tel.: +82 2 880 1941; fax: +82 2 882 0561.
E-mail address: kyi@snu.ac.kr (K. Yi).

Nomenclature

a	distance from the center of gravity (CG) to the front axle	F_{yf}	lateral tire force of the front side
a_y	lateral acceleration of the vehicle	F_{yr}	lateral tire force of the rear side
$a_{y,des}$	desired lateral acceleration	$F_{y,1}$	lateral tire force of the front-left wheel
$a_{y,c}$	critical lateral acceleration	F_{zf}	vertical tire force of the front side
$a_{y,m}$	sensor measurement of the lateral acceleration	F_{zr}	vertical tire force of the rear side
b	distance from CG to the rear axle	$F_{z,1}$	vertical tire force of the front-left wheel
m	vehicle mass	$F_{z,2}$	vertical tire force of the front-right wheel
t	tread (track width)	$F_{z,3}$	vertical tire force of the rear-left wheel
v_x	longitudinal velocity of the vehicle	$F_{z,4}$	vertical tire force of the rear-right wheel
$v_{x,des}$	desired longitudinal velocity of the vehicle	I_z	moment of inertia about the yaw axis
v_y	lateral velocity of the vehicle	M_z	direct yaw moment
C_f	cornering stiffness of the front tire	β	side slip angle of the vehicle
C_r	cornering stiffness of the rear tire	δ_f	tire steer angle
F_x	longitudinal tire force	ϕ	vehicle roll angle
$F_{x,1}$	longitudinal tire force of the front-left wheel	ϕ_{th}	roll angle threshold
F_{xf}	longitudinal tire force of the front side	$\dot{\phi}$	vehicle roll rate
F_{xy}	longitudinal tire force of the rear side	ϕ_{th}	roll rate threshold
		γ	yaw rate
		γ_d	desired yaw rate

dominant factor in vehicle rollover, much research into rollover prevention has proposed the use yaw motion control to reduce the lateral acceleration. However, since these rollover prevention schemes only focus on reducing the lateral acceleration, vehicle maneuverability and lateral stability cannot be guaranteed (Yoon, Cho, Koo, & Yi, 2009). For instance, when the rollover prevention controller works to reduce the lateral acceleration, this tends to be in the opposite direction to the intentions of the driver which may cause the vehicle to deviate from the road, thereby resulting in an accident. Studies have been conducted to prevent rollover while maintaining good lateral stability. Jo et al. proposed a VDC system for rollover prevention and ensuring lateral stability (Jo, You, Jeong, Lee, & Yi, 2008). In this research, a VDC is designed and activated – in descending order of priority – rollover prevention, excessive side-slip angle, and under-steering/over-steering of the vehicle. However, this method leads to reduction of the maneuverability or rollover prevention.

For this reason, the unified chassis control (UCC) algorithm has been designed to prevent vehicle rollover while, at the same time, ensuring good maneuverability and lateral stability by integrating individual chassis control modules, such as ESC and active front steering (AFS). A vehicle speed control algorithm has been designed to prevent rollover and an algorithm for controlling the yaw motion has been designed to improve the maneuverability and the lateral stability. The proposed UCC works to enhance the maneuverability and the lateral stability in normal driving situations without danger of rollover. When the risk of rollover increases, the proposed UCC works to prevent vehicle rollover and at the same time ensures the vehicle can continuously move in the path intended by the driver. In order to detect an impending vehicle rollover, the rollover index (RI), as proposed in a prior study (Yoon et al., 2007), is employed.

Since the UCC controller always works with the driver, the overall vehicle performance will depend not only on how well the controller works but also on its interactions with the human driver. Therefore, a closed human-in-the-loop evaluation would be a more effective way of designing the UCC controller than performing open-loop simulations that use the prescribed steering and velocity profiles (Chung & Yi, 2006). Moreover, the evaluation of active safety systems, such as UCC, active cruise control, collision warning, collision avoidance, etc., rely heavily on field testing that entails time-consuming and expensive trials, and

often significant danger (Han & Yi, 2006a). A model-based simulation makes it possible to perform exhaustive design trials and evaluations prior to field testing. For this reason, a full-scale driving simulator on a virtual test track (VTT) has been developed and used in a human-in-the-loop evaluation of the UCC where the VTT, based on the concept of rapid control prototyping (RCP), has been described in Lee (2004).

In this paper, the control performance of the proposed UCC algorithm has been investigated by a real-time human-in-the-loop simulation, using a vehicle simulator on a VTT. The tests, based on the VTT, are conducted by thirteen drivers and the results have been analyzed in detail and summarized here.

2. Unified chassis controller design

In this study, the UCC system is designed to prevent a vehicle rollover and to improve both the maneuverability and the lateral stability of the vehicle by integrating the individual chassis control modules such as the ESC and AFS. There are three control modes, namely, **ROM**, **ESC- γ** , and **ESC- β** , which stand for rollover prevention, maneuverability and lateral stability, respectively. The proposed UCC works to enhance the maneuverability and the lateral stability in normal situations without danger of rollover. The improvement in maneuverability and lateral stability is achieved by reducing the yaw rate error between the actual yaw rate and the desired yaw rate, based on the driver's steering input and the vehicle's side slip angle. When the risk of rollover is high, the proposed UCC works to reduce vehicle rollover and, at the same time, improves the maneuverability and the lateral stability. As mentioned in the previous section, since prior research concerning rollover mitigation (ROM) control, i.e., an RI-based ROM control (Yoon et al., 2007), is only focused on the prevention of vehicle rollover, then vehicle maneuverability and lateral stability cannot be guaranteed. For instance, since vehicle rollover generally occurs at large lateral accelerations, prior RI-based ROM controllers operate to reduce the lateral acceleration. This control strategy tends to control the vehicle in the opposite direction intended by the driver which may cause the vehicle to deviate from the road resulting in accidents. For this reason, an RI/vehicle stability (VS)-based UCC controller is designed to prevent

vehicle rollover and at the same time ensuring that the vehicle can continuously move in the intended path of the driver.

Fig. 1 shows a schematic diagram of the RI/VS-based UCC strategy where the proposed UCC system consists of upper and lower-level controllers where the upper-level controller determines the control mode, such as rollover prevention, maneuverability level, and lateral stability; it also calculates the desired braking force and the desired yaw moment for its objectives. Each control mode generates a control yaw moment

$$\begin{cases} RI = C_1 \left(\frac{|\phi(t)|\dot{\phi}_{th} + |\dot{\phi}(t)|\phi_{th}}{\phi_{th}\dot{\phi}_{th}} \right) + C_2 \left(\frac{|a_y|}{a_{y,c}} \right) + (1 - C_1 - C_2) \left(\frac{|\phi(t)|}{\sqrt{(\phi(t))^2 + (\dot{\phi}(t))^2}} \right), & \phi(\dot{\phi} - k_1\phi) > 0 \\ RI = 0, & \phi(\dot{\phi} - k_1\phi) \leq 0 \end{cases} \quad (1)$$

and a longitudinal tire force in line with its coherent objective. The lower-level controller calculates the longitudinal and lateral tire forces as inputs of the control modules, such as the ESC and the AFS.

2.1. The upper-level controller: decision, desired braking force, and desired yaw moment

The upper-level controller consists of three control modes and a switching logic. A control yaw moment and the longitudinal tire force are determined in line with its coherent control mode so that the switching across control modes is performed on the basis

of the threshold. Based on the driver’s input and sensor signals, the upper-level controller determines which control mode is to be selected, as shown in Fig. 2.

In this study, RI is used to detect an impending vehicle rollover where the RI is a dimensionless number that can indicate the risk of vehicle rollover and it is calculated through: the measured lateral acceleration, a_y , the estimated roll angle, ϕ , the estimated roll rate, $\dot{\phi}$, and their critical values which depend on the vehicle geometry in the following manner (Yoon et al., 2007):

In (1), C_1 , C_2 , and k_1 are positive constants ($0 < C_1 < 1$, $0 < C_2 < 1$), C_1 and C_2 are weighting factors, which are related to the roll states and the lateral acceleration of the vehicle, and k_1 is a design parameter which is determined by the roll angle-rate phase plane analysis. These parameters in (1) are determined through a simulation study undertaken under various driving situations and tuned such that an RI of 1 indicates wheel-lift-off. A detailed description for the determination of the RI is provided in previous research (Yoon et al., 2007). The lateral acceleration can easily be measured from sensors that already exist on a vehicle equipped with an ESC system. However, additional sensors are needed to measure the roll angle and the roll rate, although it is difficult and costly to directly measure these (Schubert, Nichols,

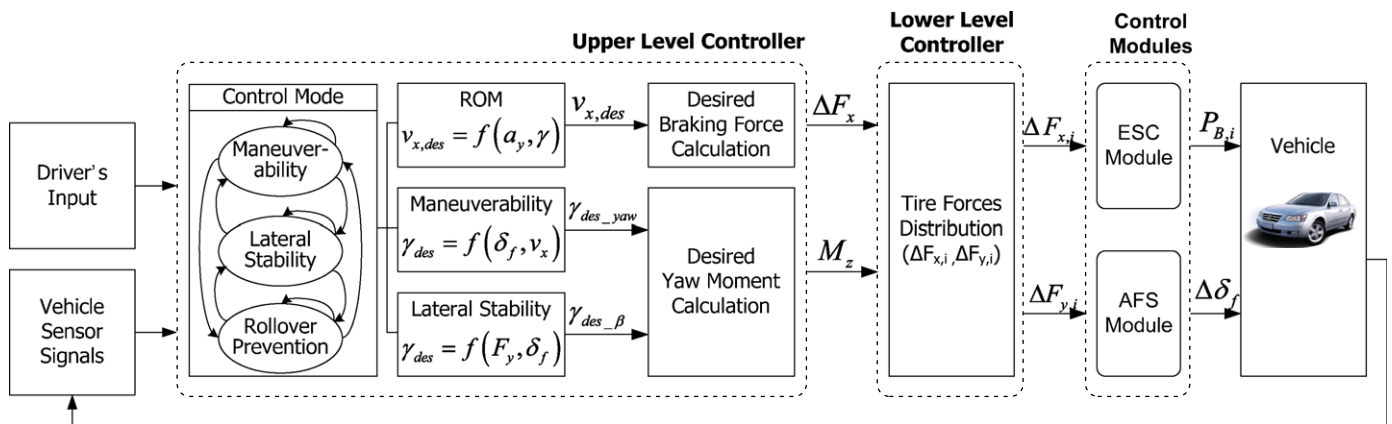


Fig. 1. RI/VS-based UCC strategy.

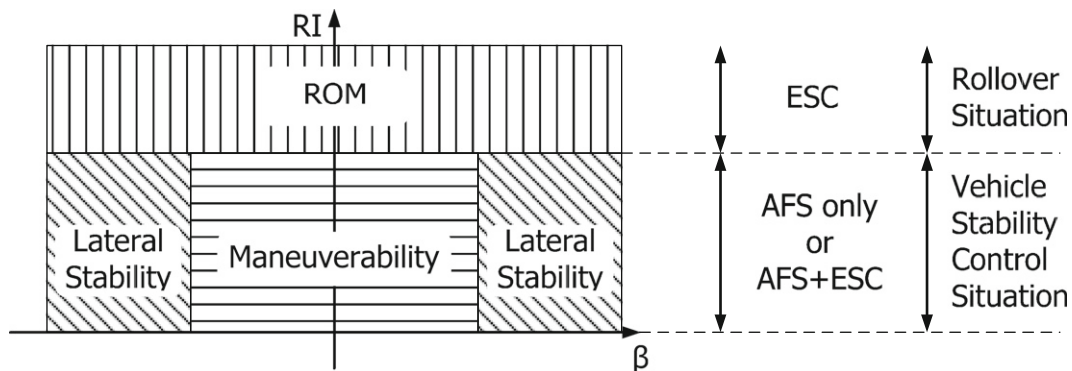


Fig. 2. Control modes for the proposed UCC system.

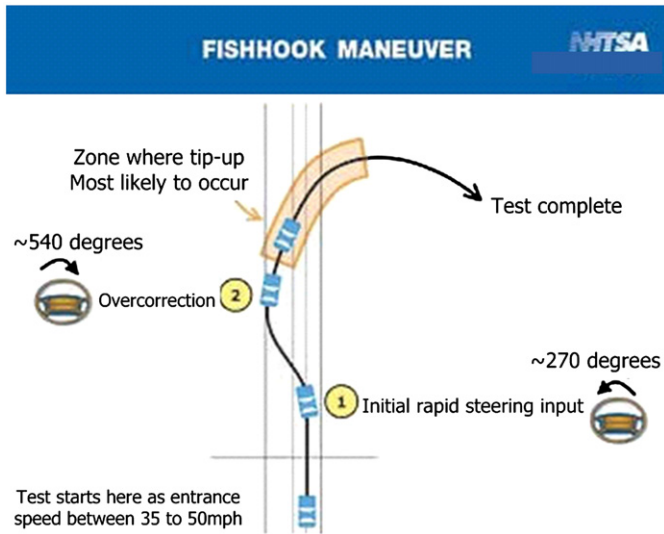


Fig. 3. Fishhook maneuver developed by NHTSA (adopted from Corrsys-Datron).

Wallner, Kong, & Schiffmann, 2004). For this reason, the roll angle and the roll rate are estimated by a model-based roll state estimator (Park, Yoon, Yi, & Kim, 2008).

The proposed *RI* is evaluated using vehicle test data obtained from the MANDO Corporation. Note that the test data used in this evaluation are not the outcome from the proposed UCC system. In other words, the control algorithm of MANDO is different from the one described in this paper so that the test results show little difference compared with the desired results. Fig. 4 shows the vehicle test data and the rollover index for the fishhook test which has been developed by NHTSA, as a dynamical test for the prediction of dynamic rollover propensity and the test results are used for vehicle evaluation. The fishhook test maneuver is described in Fig. 3.

Fig. 4(a) shows the time histories of the steering angle of two test cases where the entrance speeds are 43.2 and 45.6 mph, respectively, but the vehicle stability control input is applied only for the 45.6 mph case. In both cases, either one or two wheels are lifted off at about 4.2 s, and the rollover indices increase over unity. However, once the control input is selected, the roll angle and the lateral acceleration are decreased, and the rollover index also decreases below unity, as shown in Fig. 4(b)–(d). In contrast with the control case, the roll angle, the lateral acceleration, and the rollover index increase over unity in the non-control case. Consequently, the vehicle is rolled over at about 6 s.

If the *RI* exceeds a particular threshold, then the rollover prevention mode, **ROM**, is activated, otherwise, the controller is in either the maneuverability mode or in the lateral stability mode. Under a small side slip angle, the controller is in the maneuverability mode, **ESC- γ** , if the error between the actual yaw rate and the desired yaw rate exceeds a particular threshold. The condition of activation of the lateral stability mode is determined by the vehicle side slip angle. If the side slip angle exceeds the threshold value, the controller is in the lateral stability mode, **ESC- β** and the side slip angle can be successfully estimated in real time from already existing vehicle sensors (You, Hahn, & Lee, 2009).

The maneuverability and the lateral stability are ensured by the yaw moment control method and rollover prevention is achieved by the yaw moment/speed control. The upper-level controller calculates the desired braking force, ΔF_x , for rollover prevention and the desired yaw moment, M_z , for maneuverability and lateral stability. The state-transition diagram for the required

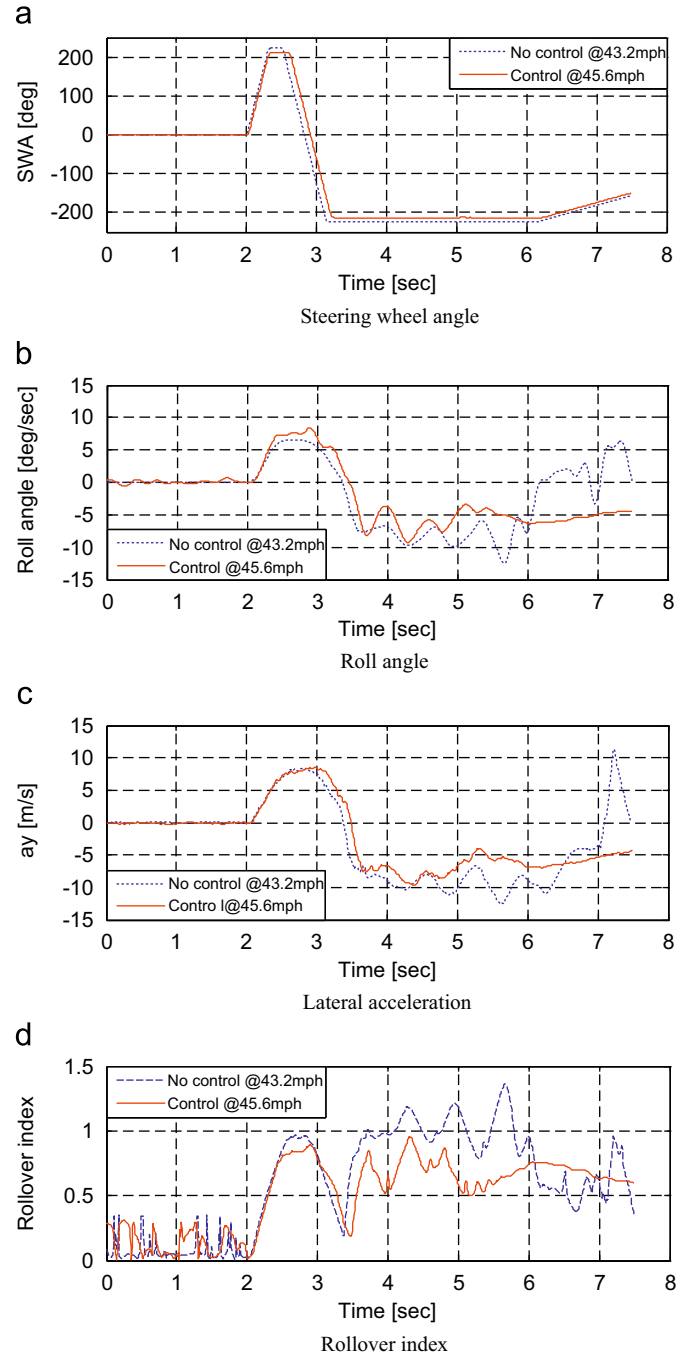


Fig. 4. Rollover index validation through vehicle test data (NHTSA fishhook test).

control mode switching in the upper-level controller is given in Fig. 5.

The signals used for the state transitions are the yaw rate error, γ_e , the side slip angle, β , and the *RI* so that each event in Fig. 5 represent a switching condition, and the conditions of its activation are described in Table 1. When the vehicle state is either **ESC- γ** or **ESC- β** , as shown in Fig. 5, the yaw moment control is applied and generates the desired yaw moment to track a target yaw rate. In **ESC- γ** , a target yaw rate is generated on the basis of the driver's steering input for maneuverability and in **ESC- β** , a target yaw rate is generated to reduce some excessive side slip angle, β , for achieving lateral stability. When the vehicle state is **ROM**, the yaw moment and speed control are applied to generate

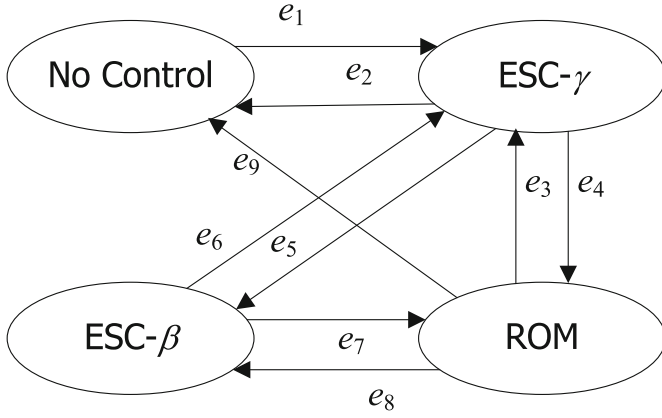


Fig. 5. State-transition diagram for the control mode switching.

Table 1
Events and corresponding conditions of activation.

Events	Activation condition
e_1	$ \gamma_e \geq \gamma_{e_threshold}$
e_2	$ \gamma_e < \gamma_{e_threshold}$
e_3	$RI < RI_{threshold}$
e_4	$RI \geq RI_{threshold}$
e_5	$RI < RI_{threshold}, \beta \geq \beta_{threshold}$
e_6	$RI < RI_{threshold}, \beta < \beta_{threshold}, \gamma_e \geq \gamma_{e_threshold}$
e_7	$RI \geq RI_{threshold}, \beta \geq \beta_{threshold}$
e_8	$RI < RI_{threshold}, \beta \geq \beta_{threshold}$
e_9	$RI < RI_{threshold}, \beta < \beta_{threshold}, \gamma_e < \gamma_{e_threshold}$

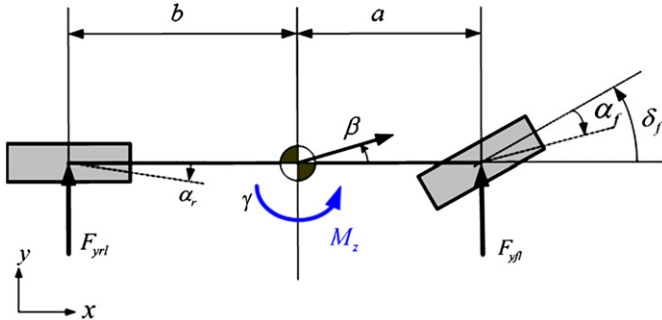


Fig. 6. A 2-D bicycle model including the direct yaw moment.

the desired yaw moment for vehicle stability and the braking force for rollover prevention, respectively.

In Table 1, The $RI_{threshold}$ is set to 0.7, which is the critical value at which all the wheels of the vehicle contact with the ground and the $\beta_{threshold}$ is selected as 0.06 rad under the assumption of $\mu=0.3$ from the literature (Rajamani, 2006). The threshold for the yaw rate error $\gamma_{e,th}$ is set to 0.08 rad/s to give the largest yaw rate error when the vehicle is performing a single lane change at 60 km/h on dry asphalt.

2.1.1. Desired yaw moment for maneuverability and lateral stability (ESC- γ /ESC- β modes)

If the RI is small, the **ESC- γ** or the **ESC- β** mode is activated for achieving the desired maneuverability or lateral stability, respectively. In this control mode, the desired yaw moment is determined whose purpose is to reduce the yaw rate error by using a bicycle model for computing the target vehicle response. This linear model can represent the vehicle dynamics in the

region of linear tire characteristics, and has been validated in many publications in the literature (see for example, Nagai, Shino, & Gao, 2002). In addition, since the vehicle active safety control should be intervened before the vehicle enters any dangerous situations in which the tires are near the limits of adhesion, the characteristic of the tire is beyond the linear region at that time when the control intervention is needed. Hence, the linear bicycle model is sufficient to design a controller to ensure vehicle stability.

A direct yaw moment control method is employed to determine the desired yaw moment and Fig. 6 shows the 2-D bicycle model, including the direct yaw moment, M_z .

The dynamic equations of the 2-D bicycle model are represented as follows:

$$\begin{bmatrix} \dot{\beta} \\ \dot{\gamma} \end{bmatrix} = \begin{bmatrix} \frac{-2(C_f + C_r)}{mv_x} & \frac{2(-aC_f + bC_r)}{mv_x^2} - 1 \\ \frac{2(-aC_f + bC_r)}{I_z} & \frac{-2(a^2C_f + b^2C_r)}{I_z v_x} \end{bmatrix} \begin{bmatrix} \beta \\ \gamma \end{bmatrix} + \begin{bmatrix} \frac{2C_f}{mv_x} \\ \frac{2aC_f}{I_z} \end{bmatrix} \Delta_f + \begin{bmatrix} 0 \\ \frac{1}{I_z} \end{bmatrix} M_z \quad (2)$$

In general, through Eq. (2), the desired yaw rate, based on the driver's steering input, is theoretically determined in light of the 2-D bicycle model with a linear tire force. The steady-state yaw rate of the bicycle model is introduced and the maneuver of the vehicle is considered to reflect the driver's intentions and this is expressed as a function of the vehicle's longitudinal velocity and the driver's steering input, as follows:

$$\gamma_{des_yaw} = \frac{1}{1 - ((m(aC_f - bC_r)v_x^2) / (2C_f C_r (a + b)^2))} \frac{v_x}{a + b} \Delta_f \quad (3)$$

The desired yaw rate, which is represented in (3), is used as the reference yaw rate for the **ESC- γ** control mode.

In general, the lateral stability cannot be guaranteed if the side slip angle exceeds about 3° and excessive body side slip of a vehicle causes its yaw motion to be insensitive to the driver's steering input and threatens the lateral stability. As the side slip angle of a vehicle increases, the stabilizing yaw moment due to the steering input decreases, and thus, the lateral behavior of the vehicle becomes unstable. Therefore, a control intervention to maintain the body side slip angle to lie within a reasonably small range, i.e., 3° , is required to improve the lateral stability of the vehicle (Jo et al., 2008).

Through a 2-D bicycle model, the lateral vehicle dynamics are expressed as follows:

$$m\dot{v}_y = -mv_x\gamma + 2F_{yf} \cos \Delta_f + 2F_{yr} \quad (4)$$

From (4), assuming that $\dot{v}_x \approx 0$, the side slip angle dynamics can be expressed as follows:

$$\dot{\beta} = -\gamma + \frac{2F_{yf} \cos \Delta_f + 2F_{yr}}{mv_x} \quad (5)$$

Let the desired yaw rate be defined as

$$\gamma_{des_lateral} = K_1\beta + \frac{2F_{yf} \cos \Delta_f + 2F_{yr}}{mv_x} \quad (6)$$

Then, the dynamics of the body side slip angle are stable, as shown in (7), which implies that the body sideslip angle asymptotically converges to zero:

$$\dot{\beta} = -K_1\beta \quad (7)$$

In (7), K_1 is a design parameter, which is strictly positive. The desired yaw rate, which is represented in (6), is used as the reference yaw rate for the **ESC- β** control mode and the reference yaw rate, γ_{des} , for determining the desired yaw moment is selected through either (3) or (6), depending on the control mode.

The desired yaw moment can be obtained through (2) and the reference yaw rate, which is one of (3) and (6). From (2), the dynamic equation concerning the yaw rate, including the direct yaw moment, is presented as follows:

$$\dot{\gamma} = \frac{2(-aC_f + bC_r)}{I_z} \beta + \frac{-2(a^2C_f + b^2C_r)}{I_z v_x} \gamma + \frac{2aC_f}{I_z} \Delta_f + \frac{1}{I_z} M_z \quad (8)$$

The sliding mode control method has also been used to determine the desired yaw moment; in this the sliding surface and the sliding condition are defined as follows:

$$s_1 = \gamma - \gamma_{des}, \quad \frac{1}{2} \frac{d}{dt} s_1^2 = s_1 \dot{s}_1 \leq -\eta_1 |s_1| \quad (9)$$

where η_1 is a positive constant. The equivalent control input that would achieve $\dot{s}_1 = 0$ is calculated as follows:

$$M_{z,eq} = -I_z \left(\frac{2(-a\hat{C}_f + b\hat{C}_r)}{I_z} \beta - \frac{2(a^2\hat{C}_f + b^2\hat{C}_r)}{I_z v_x} \gamma + \frac{2a\hat{C}_f}{I_z} \Delta_f \right) \quad (10)$$

Finally, the desired yaw moment for satisfying the sliding condition regardless of the model uncertainty is determined as follows:

$$M_z = M_{z,eq} - K_2 \text{sat} \left(\frac{\gamma - \gamma_{des}}{\Phi_1} \right) \quad (11)$$

where Φ_1 is a control boundary, and the gain, K_2 , which satisfies the sliding condition, is calculated as follows:

$$K_2 = I_z \left\{ \frac{F_{yf}}{I_z} |-a\beta - a^2\gamma + a\Delta_f| + \frac{F_{yr}}{I_z} |b\beta - b^2\gamma| + |\dot{\gamma}_{des}| + \eta_2 \right\} \quad (12)$$

2.1.2. Desired braking force for rollover prevention (the ROM mode)

If the *RI* increases to a predefined *RI* threshold value, which can predict an impending rollover, the ROM control input should be applied to the vehicle in order to prevent rollover. Rollover prevention control can be achieved through vehicle speed control and the desired braking force is determined in this section to control the speed. In addition, the desired yaw moment, as determined in the previous section, is also applied to the vehicle to improve the maneuverability and the lateral stability.

As mentioned previously, since vehicle rollovers occur at large lateral accelerations, the desired lateral acceleration should be defined and can be determined from the *RI* (cf. Eq. (1)) as follows:

$$a_{y,des} = \frac{1}{C_2} \left\{ RI_{tar} - C_1 \left(\frac{|\phi(t)|\dot{\phi}_{th} + |\dot{\phi}(t)|\phi_{th}}{\phi_{th}\dot{\phi}_{th}} \right) - (1 - C_1 - C_2) \left(\frac{|\phi(t)|}{\sqrt{(\phi(t))^2 + (\dot{\phi}(t))^2}} \right) \right\} a_{y,c} \quad (13)$$

In (2), the target *RI* value, RI_{tar} , is set to 0.6.

The desired vehicle speed for obtaining the desired lateral acceleration is calculated from the lateral vehicle dynamics as follows (Yoon et al., 2009):

$$v_{x,des} = \frac{1}{\gamma} \{ a_{y,des} - (a_{y,m} - v_x \gamma) \} \quad (14)$$

The desired braking force to yield the desired vehicle speed is calculated through a planar model, as shown in Fig. 7, and through the sliding mode control law.

Fig. 7 shows a planar vehicle model including the desired braking force, ΔF_x and the dynamic equation for the *x*-axis is described as follows:

$$m\dot{v}_x = F_{xr} + F_{xf} \cos \Delta_f - F_{yf} \sin \Delta_f + m v_y \gamma - \Delta F_x \quad (15)$$

By the assumption of having small steering angles, Eq. (15) can be rewritten in terms of the derivative of the vehicle speed as

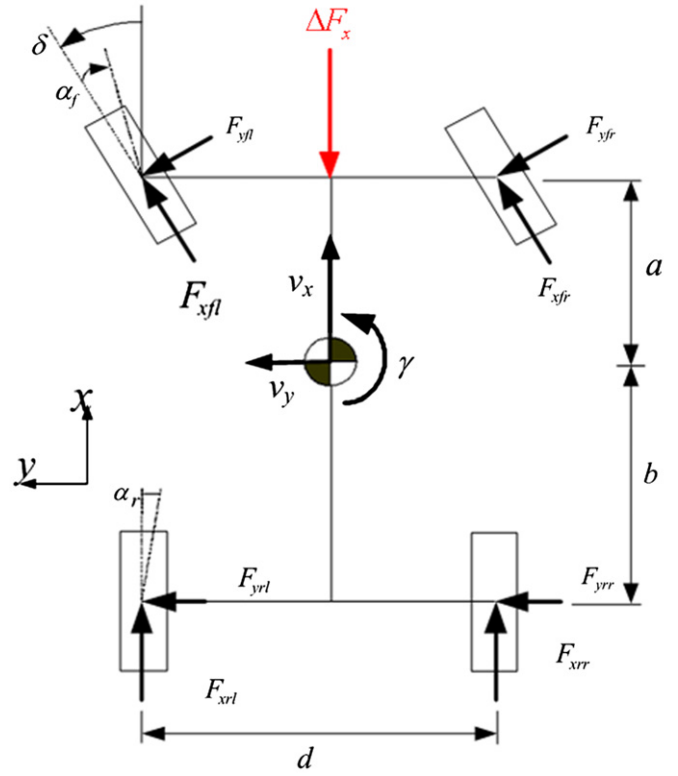


Fig. 7. Planar model including the desired braking force.

follows:

$$\dot{v}_x = \frac{1}{m} (F_{xr} + F_{xf} - F_{yf} \Delta_f) + v_y \gamma - \frac{1}{m} \Delta F_x \quad (16)$$

In order to obtain the desired braking force, the sliding mode control method is used. The sliding surface and the sliding condition are defined as follows:

$$s_2 = v_x - v_{x,des}, \quad \frac{1}{2} \frac{d}{dt} s_2^2 = s_2 \dot{s}_2 \leq -\eta_2 |s_2| \quad (17)$$

where η_2 is a positive constant.

Finally, the desired braking force for preventing a rollover is obtained as follows:

$$\Delta F_x = \Delta F_{x,eq} - K_3 \text{sat} \left(\frac{v_x - v_{x,des}}{\Phi_2} \right), \quad K_3 = -\eta_2 m \quad (18)$$

where $\Delta F_{x,eq} = (F_{xf} + F_{xr} - F_{yf} \Delta_f) + m(v_y \gamma - \dot{v}_{x,des})$. In (18), Φ_2 is a control boundary to eliminate high signal chattering due to high frequency components in the control input. Further information about the desired braking force can be found in previous research (Yoon et al., 2009).

2.2. The lower-level controller

The lower-level controller distributes the desired braking force and the yaw moment to the longitudinal and lateral tire forces as inputs of the ESC and AFS modules. In this paper, two schemes are used to distribute the desired braking force and the yaw moment. One is an optimized distribution scheme without any risk of causing rollover, and the other is a simple distribution scheme that has risk of rollover. The former is used in the **ESC- γ** and **ESC- β** modes, while the latter is used in the **ROM** mode. The optimized distribution scheme determines the differential braking input and active front steering input for the ESC and AFS modules, respectively. This optimization problem focuses on minimizing the use of braking because the ESC module has some negative

effects as the simple distribution scheme determines only the differential braking input for the ESC module. These two schemes are switched in accordance with the protocol for switching across control modes in the upper-level controller and the only ESC module is used in the **ROM** mode since the optimized distribution scheme for the AFS and ESC modules provides a very small braking to each wheel, which cannot decrease the vehicle speed which is essential for preventing rollover.

Moreover, the slip angle of the tire is proportionally increased with the lateral acceleration as shown in Fig. 8. Since vehicle

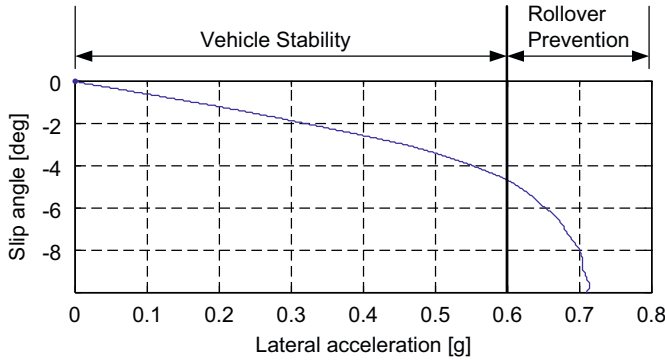


Fig. 8. Relation between the lateral acceleration and the slip angle.

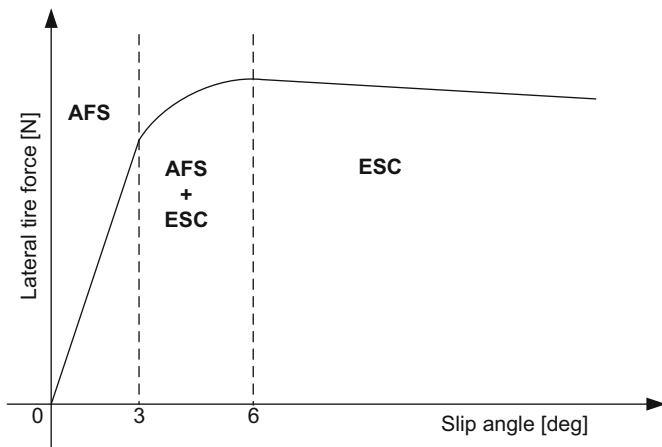


Fig. 9. Characteristics of the lateral tire force.

rollovers generally occurs at large lateral acceleration, the slip angle of the tire is also very large in the **ROM** mode situation.

The AFS module cannot generate the lateral tire force in large slip angle situations as shown in Fig. 9; therefore the AFS module is not used in the **ROM** mode, that is, the ESC is the most effective for the **ROM** mode. For this reason, only the ESC control module is used for the **ROM** mode.

2.2.1. Tire-force distribution in vehicle stability situations (ESC- γ /ESC- β mode)

In vehicle stability situations that do not have risk of rollover, the control interventions for maneuverability, **ESC- γ** , and for lateral stability, **ESC- β** , are activated. When the lateral acceleration is small enough so that the slip angle is small, the characteristics of the lateral tire force lie within the linear region, as shown in Fig. 9. In these situations, only the AFS control module is applied and the AFS control input is determined through the consideration of the 2-D bicycle model as follows:

$$\Delta\delta_f = \frac{M_z}{2aC_f} \tag{19}$$

When the lateral acceleration increases greatly, the combined control inputs that are based on the ESC and AFS modules are applied. Since the ESC module has some negative effects, such as the degradation of ride comfort and the wear of tires and brakes, the optimized coordination of tire forces is focused on minimizing the use of braking. An optimal coordination of the lateral and longitudinal tire forces for the desired yaw moment is determined through the Karush–Kuhn–Tucker (KKT) conditions (Cho, Yoon, & Yi, 2007). Fig. 10 shows the coordinate system corresponding to the resultant force when the desired yaw moment is positive.

The sign of the desired yaw moment determines what tire forces should be used for optimal coordination. If the desired yaw moment is positive, four variables, ΔF_{x1} , ΔF_{y1} , ΔF_{y2} , and ΔF_{x3} , should be coordinated to generate the yaw moment as represented in Fig. 10.

These optimal variables can be reduced by using some relations which correspond to the vertical load of the vehicle. Since the active steering angles for both front tires are the same, the active lateral tire forces have a relation as follows:

$$\Delta F_{y2} = \frac{F_{z2}}{F_{z1}} \Delta F_{y1} \tag{20}$$

Moreover, the longitudinal tire forces at the front and rear have a relation as follows:

$$\Delta F_{x3} = \frac{F_{z3}}{F_{z1}} \Delta F_{x1} \tag{21}$$

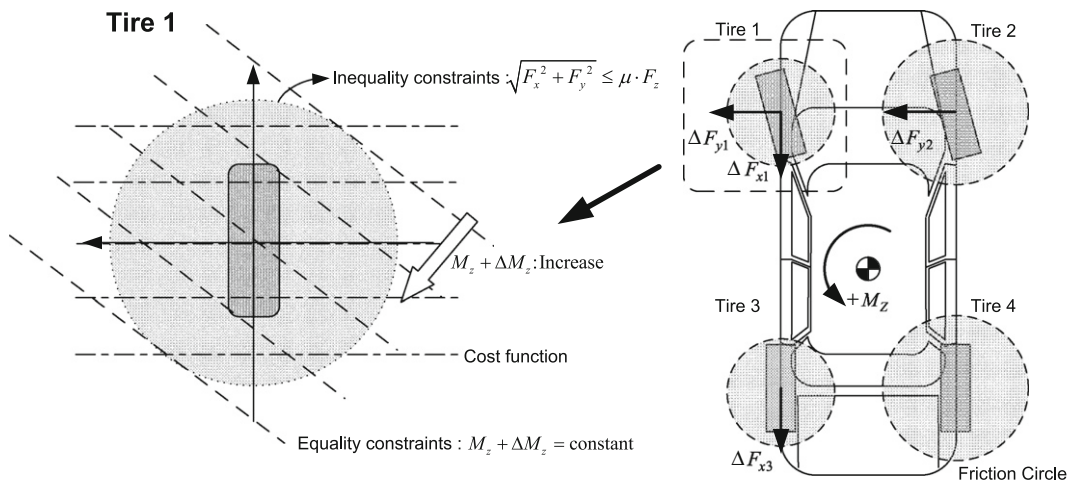


Fig. 10. Coordinate system corresponding to the resultant force ($M_z > 0$).

Using (20) and (21), two variables, ΔF_{y2} and ΔF_{x3} , can be eliminated in the optimization problem so that the optimal distribution problem for the longitudinal and lateral tire forces involves only two variables, namely, ΔF_{x1} and ΔF_{y1} .

The cost function of the proposed optimization is the magnitude of the additional longitudinal tire force by braking as follows:

$$L(\Delta F_x) = \Delta F_{x1}^2 \tag{22}$$

This optimization problem has the two variables, ΔF_{x1} and ΔF_{y1} , along with equality and inequality constraints; two of these constraints are determined as follows:

$$f(x) = -\frac{t}{2}D_1\Delta F_{x1} + aD_2\Delta F_{y1} - M_Z = 0 \tag{23}$$

$$g(x) = (\Delta F_{x1} + F_{x1})^2 + (\Delta F_{y1} + F_{y1})^2 - \mu^2 F_{z1}^2 \leq 0 \tag{24}$$

In the above, $D_1 = 1 + (F_{z3}/F_{z1})$, $D_2 = 1 + (F_{z2}/F_{z1})$. The equality constraint in (23) means that the sum of the yaw moment generated by the longitudinal and the lateral tire forces should be equal to the desired yaw moment. The inequality constraint in (24) means that the sum of the longitudinal and the lateral tire forces should be less than the friction forces on the tire.

From (22)–(24), the Hamiltonian is defined as follows:

$$H = \Delta F_{x1}^2 + \lambda \left(-\frac{t}{2}D_1\Delta F_{x1} + aD_2\Delta F_{y1} - M_Z \right) + \rho \left((\Delta F_{x1} + F_{x1})^2 + (\Delta F_{y1} + F_{y1})^2 - \mu^2 \cdot F_{z1}^2 + c^2 \right) \tag{25}$$

where λ is the Lagrange multiplier, c the slack variable, and ρ the semi-positive number.

First-order necessary conditions about the Hamiltonian are determined by the Karush–Kuhn–Tucker condition theory as follows:

$$\frac{\partial H}{\partial \Delta F_{x1}} = 2\Delta F_{x1} - \frac{t}{2}D_1\lambda + 2\rho(\Delta F_{x1} + F_{x1}) = 0 \tag{26}$$

$$\frac{\partial H}{\partial \Delta F_{y1}} = aD_2\lambda + 2\rho(\Delta F_{y1} + F_{y1}) = 0 \tag{27}$$

$$\frac{\partial H}{\partial \lambda} = -\frac{t}{2}D_1\Delta F_{x1} + aD_2\Delta F_{y1} - \Delta M_Z = 0 \tag{28}$$

$$\rho g(x) = \rho \left((\Delta F_{x1} + F_{x1})^2 + (\Delta F_{y1} + F_{y1})^2 - \mu^2 F_{z1}^2 \right) = 0 \tag{29}$$

From (29), two cases are derived with respect to ρ and $g(x)$ as follows:

Case 1. $\rho = 0, g(x) < 0$.

Case 2. $\rho > 0, g(x) = 0$.

Case 1 means that the sum of longitudinal and lateral tire forces is smaller than the friction of the tire. On the other hand, Case 2 means that the sum of the longitudinal and lateral tire forces is equal to the friction of the tire. The solutions of the optimization problem represented in (3.41) can be obtained for both cases.

If the desire yaw moment is positive, $M_Z > 0$, the solutions are obtained as follows:

$$\text{Case 1 : } \begin{cases} \Delta F_{x1} = 0 \\ \Delta F_{y1} = \frac{M_Z}{aD_2} \end{cases} \tag{30}$$

$$\text{Case 2 : } \begin{cases} \Delta F_{x1} = \frac{-(F_{x1} + \kappa\zeta) + \sqrt{(1 + \kappa^2)\mu^2 F_{z1}^2 - (\kappa F_{x1} - \zeta)^2}}{(1 + \kappa^2)} \\ \Delta F_{y1} = \frac{tD_1}{2aD_2}\Delta F_{x1} + \frac{1}{aD_2}M_Z \end{cases} \tag{31}$$

where $\kappa = (tD_1/2aD_2)$ and $\zeta = (1/aD_2)M_Z + F_{y1}$.

The brake pressure for the ESC module and the additional steering angle for the AFS module are determined from (32)

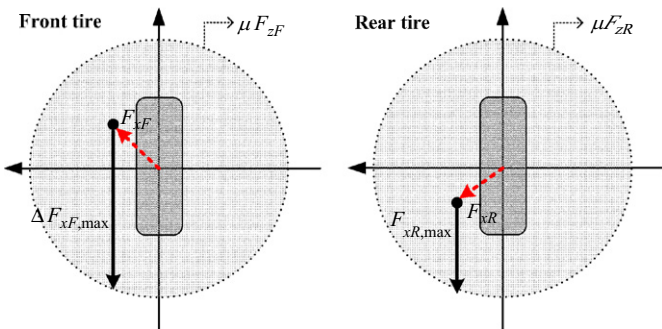


Fig. 11. Friction circles of the front and rear tires.

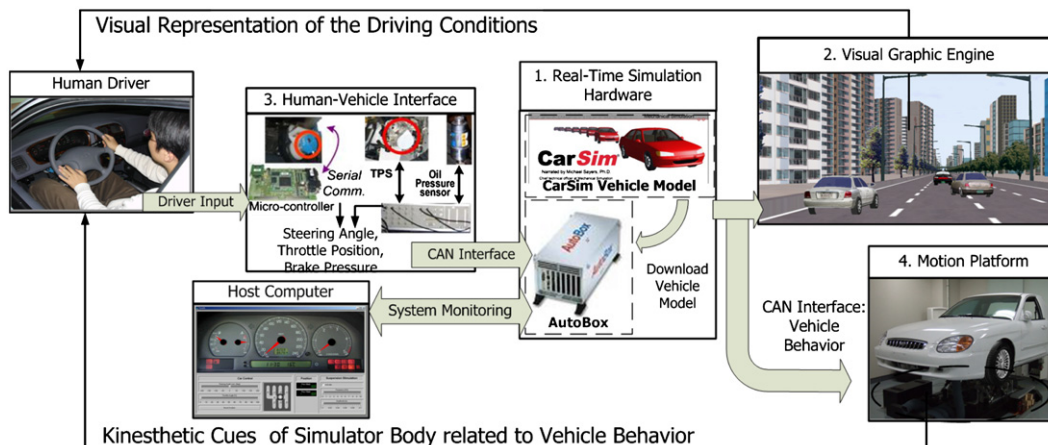


Fig. 12. Hardware configuration of the driving simulator with a human in-the-loop.

as follows:

$$\begin{cases} \Delta\Delta_f = \frac{\Delta F_{yi}}{C_f} \\ P_{Bi} = \frac{r_{wf}\Delta F_{xi}}{K_{Bi}} \end{cases} \quad (i = 1,2) \quad (32)$$

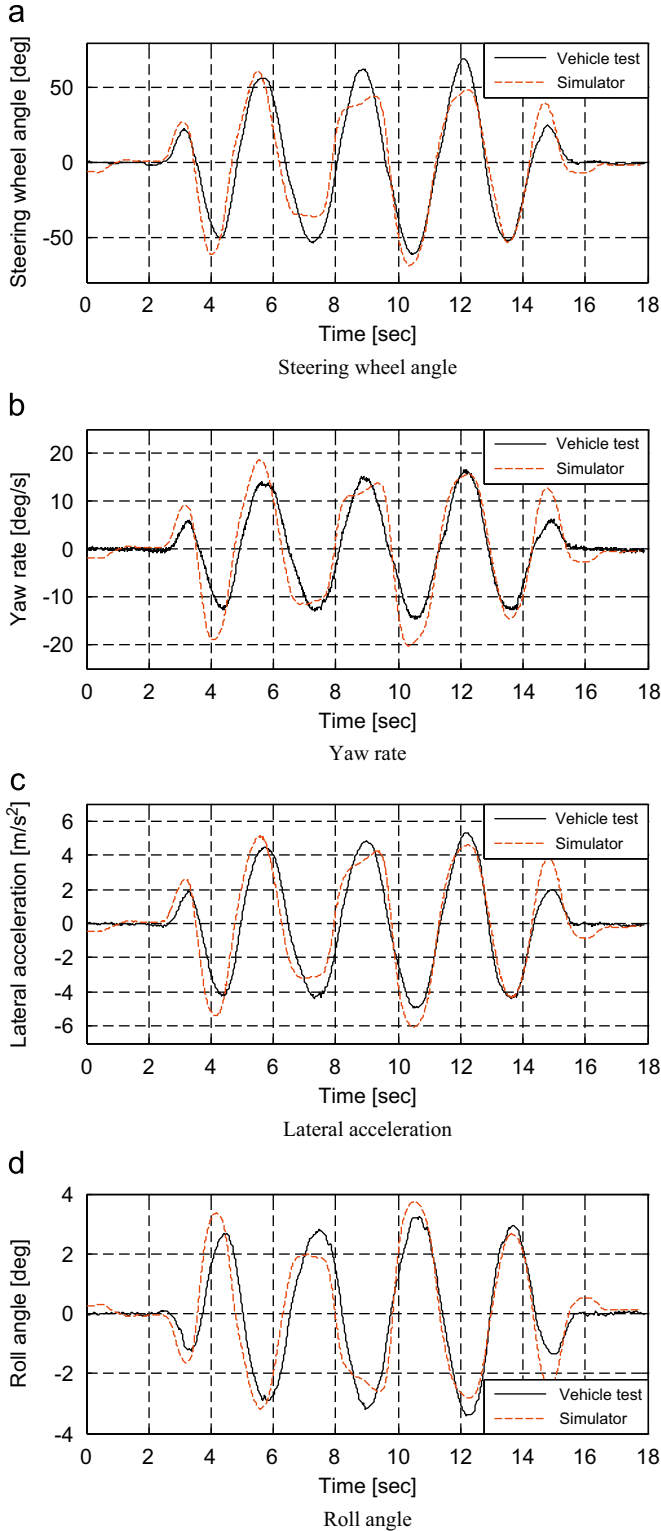


Fig. 13. Comparison between actual vehicle test data and the driving simulator (for the slalom test).

In (32), K_{Bi} is the brake gain, and r_{wf} the radius of the wheel. When the desired yaw moment is negative, $M_z < 0$, the tire forces can be obtained in a manner similar to (30) and (31).

2.2.2. Tire-force distribution in rollover situations (ROM mode)

In the previous sections, the desired braking force, which should be subjected to the vehicle for rollover prevention, and the desired yaw moment for reducing the error in the yaw rate have been determined. By utilizing the above two values, a braking-force distribution is accomplished simply to help prevent vehicle rollover, while ensuring that the vehicle follows the intended path of the driver. The forces of the vehicle can be determined kinematically, as follows:

$$\begin{cases} \Delta F_{x,left} = \frac{1}{2} \Delta F_x + \frac{M_z}{t} \\ \Delta F_{x,right} = \frac{1}{2} \Delta F_x - \frac{M_z}{t} \end{cases} \quad (33)$$

The braking forces of the left and right sides are obtained by substituting (18) and (11) into (33). Fig. 11 shows the friction circles of the front and rear tires and the traction force, determined through the shaft torque, is applied at the front tire, and the drag force is applied at the rear tire.

The maximum braking forces of the front and rear tires can be determined as follows:

$$\Delta F_{xf,max} = F_{xf} - \sqrt{(\mu F_{zf})^2 - (F_{yf})^2} \quad (34)$$

$$\Delta F_{xr,max} = -F_{xr} - \sqrt{(\mu F_{zr})^2 - (F_{yr})^2} \quad (35)$$

The braking-force distributions of the front and rear tires are achieved by using equations from (33) through to (35) as follows:

$$\Delta F_{xr,left} = \frac{|\Delta F_{xr,left,max}|}{|\Delta F_{xf,left,max}|} \Delta F_{xf,left} \quad (36)$$

$$\Delta F_{xr,right} = \frac{|\Delta F_{xr,right,max}|}{|\Delta F_{xf,right,max}|} \Delta F_{xf,right} \quad (37)$$

In the above, $\Delta F_{xf,left} + \Delta F_{xr,left} = \Delta F_{x,left}$ and $\Delta F_{xf,right} + \Delta F_{xr,right} = \Delta F_{x,right}$.

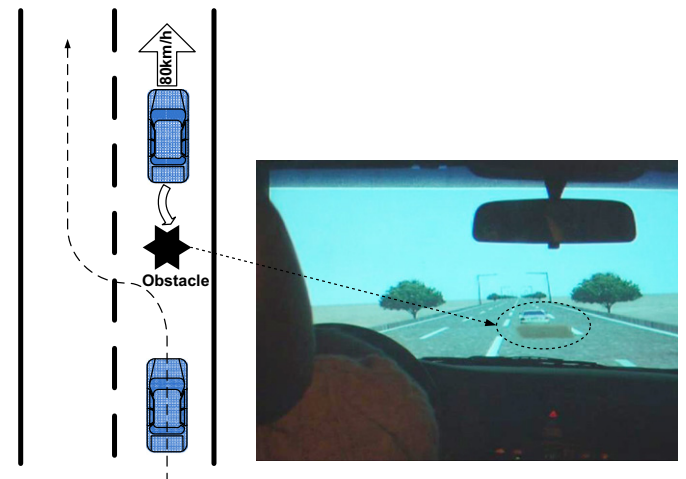


Fig. 14. The test scenario: obstacle avoidance.

The braking pressure of the front-left wheel can be determined as follows:

$$P_{Bf, \text{left}} = \begin{cases} \frac{r_{wf}(\Delta F_{xf, \text{left}})}{K_{Bf}} & \text{if } \Delta F_{xf, \text{left}} < \Delta F_{xf, \text{max}} \\ \frac{r_{wf}(\Delta F_{xf, \text{max}})}{K_{Bf}} & \text{if } \Delta F_{xf, \text{left}} \geq \Delta F_{xf, \text{max}} \end{cases} \quad (38)$$

The other tire forces can be obtained in a manner similar to (38).

3. Full-scale driving simulator

The configuration of the full-scale driving simulator for the human-in-the-loop system is shown in Fig. 12, consisting of four parts: a real-time (RT) simulation hardware, a visual graphical engine, a human-vehicle interface, and a motion platform. The host computer in Fig. 12 is utilized to modify the vehicle simulation program and to display the current vehicle status. The RT simulation hardware calculates the variables of the vehicle model represented using a CARSIM model controlled by the UCC controller with measured driver reactions. By the use of the vehicle-behavior

information obtained using RT simulation hardware, the visual graphical engine projects a visual representation of the driving conditions to the human driver via a beam projector with a 100-in screen who interacts with the 3-D virtual simulation and the kinesthetic cues of the simulator body. The driver's responses are acquired through the steering wheel angle, brake pressure, and throttle positioning sensors, as shown in Fig. 12.

The motion platform provides kinesthetic cues, which are related to the behavior of the vehicle with regard to the human driver. An actual full-sized braking system, including a vacuum booster, master cylinder, calipers, etc., is implemented in the simulator so that the feel of the braking action is similar to that of an actual vehicular brake pedal. In the case of the steering wheel, a spring and damper are used to produce the reactive forces of the steering wheel where the spring and damper characteristics are adjusted to make the feel of the steering wheel similar to that of an actual vehicle being driven in the high-speed range.

3.1. Configurations of the driving simulator

The most important feature of the driving simulator is to guarantee real-time performance and so all the subsystems are

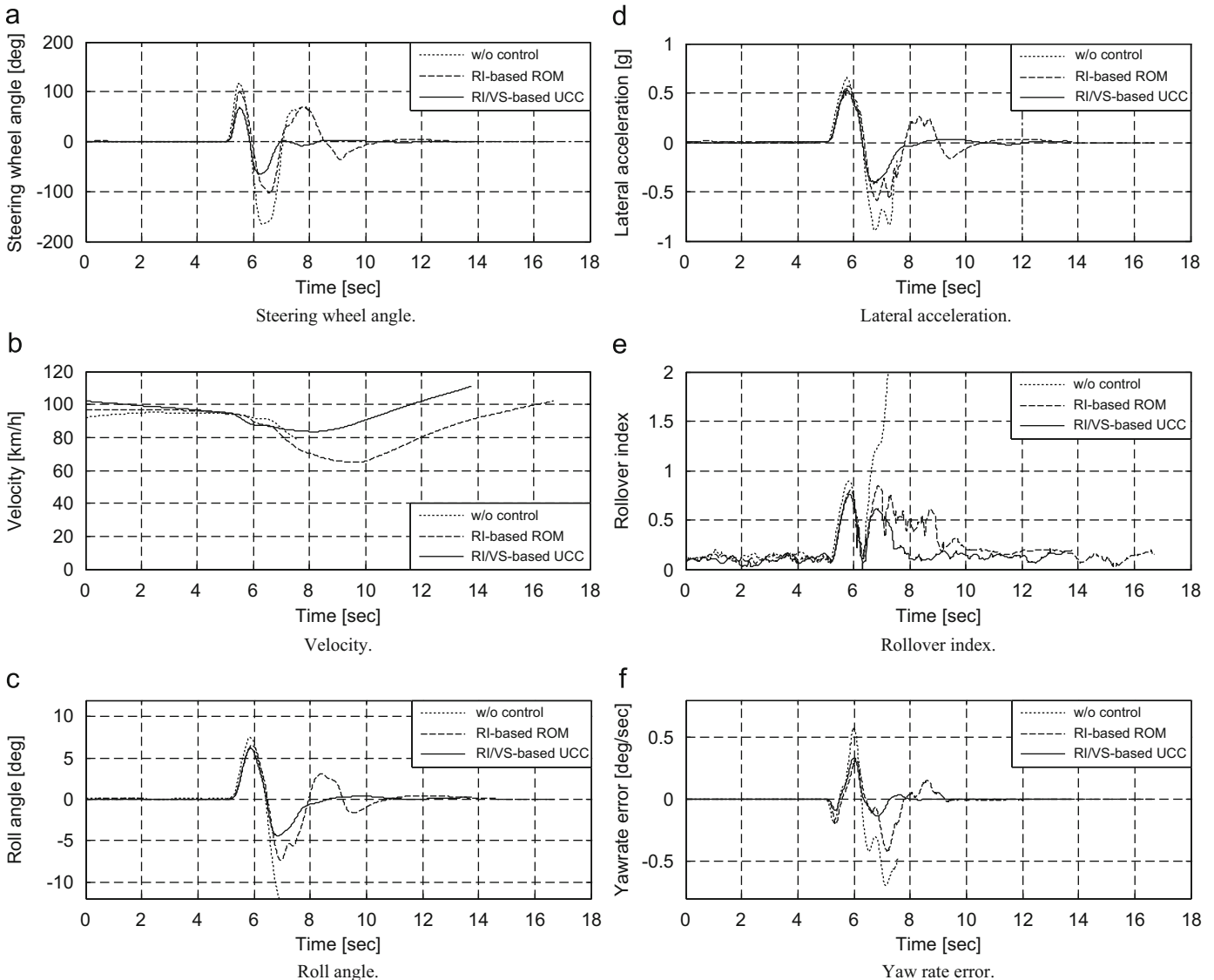


Fig. 15. Driving tests results using the full-scale simulator based on the VTT.

designed and integrated in light of achieving RT performances. The “dSPACE Autobox” environment is used as the RT simulation hardware in the driving simulator with the CARSIM, vehicle simulation software as the vehicle model (Han, Yi, & Yi, 2006).

The visual graphical engine in Fig. 12 provides a visual representation of the driving situation with the human driver and is composed of prepared 3-D model components, such as the road surface, street light, tree, guard rail, etc., in a 3-D model of a real-time simulation environment (Han & Yi, 2006b).

The human driver's inputs are measured by the brake pressure, the throttle angle and the steering angle sensors, as shown in Fig. 12. The steering angle sensor, which produces a gray code with a synchronous serial interface (SSI), is an absolute-type encoder, the throttle positioning sensor (TPS) and oil pressure sensor are installed to measure the throttle angle position and the brake pressure.

The vehicle cockpit is mounted on a 3 DOF-1000 kg electric motion platform, which applies the behavior of the vehicle model to the simulator body, as shown in Fig. 12 and the motion platform allows displacements up to a maximum of about ± 10 cm (heave) and ± 10° (roll and pitch). The motion platform renders the linear and angular accelerations of the simulated vehicle model, as computed by the RT simulation hardware so that the human driver gets an impression that s/he is driving an actual vehicle by means of the kinesthetic cues generated by the motion platform, and from the visual representation of the driving situation provided by the visual graphical engine.

3.2. Validation of the vehicle simulator

The driving simulator used in this paper is evaluated via actual vehicle test data and Fig. 13 shows the results of a slalom test in which the driver maintains an approximately constant vehicle speed of about 60 km/h. The cone width is 30 m. The magnitude and frequency of the driver's steering inputs are almost identical in both the vehicle test results and the driving simulator, as shown in Fig. 13(a). The vehicle responses in terms of the yaw rate, the lateral acceleration and the roll angle are also quite similar to the actual test results as shown in Fig. 13(b)–(d).

The comparison between the driving simulator and actual vehicle test results shows that the proposed driving simulator is feasible for describing actual vehicle dynamic behaviors. This means that the driving simulator accurately reproduces actual driving conditions.

4. Evaluation of the proposed UCC based on a VTT

Tests using the full-scale driving simulator based on the VTT have been conducted to verify the proposed RI/VS-based UCC control algorithm and its performance with that of the previous RI-based ROM control system are compared. The tests based on the VTT have been conducted by thirteen drivers, and the results are analyzed and summarized here.

The test scenario is set to the obstacle-avoidance situation shown in Fig. 14 so that when a driver follows the preceding vehicle moving at a constant speed of 90 km/h in a straight lane and an object is dropped suddenly from the preceding vehicle. In this situation, the driver abruptly steers the vehicle to avoid the dropped obstacle and the vehicle is placed in a dangerous situation. Moreover, in this extreme situation, vehicle rollover is possible and there may be a loss of maneuverability without an UCC control system.

Tests have been conducted by thirteen drivers. Fig. 15 shows the test results of the first driver, while Fig. 17 shows the vehicle's

trajectories. If the UCC control input is not applied, the vehicle rolls over in this situation. It is clear from Fig. 15(e) that the RI increases over unity in the absence of control. Further, the roll angle and lateral acceleration also increase to large values, as shown in Fig. 15(c) and (d). In addition, because this situation is very severe, the vehicle deviates from the lane, as shown in Fig. 17.

It can be seen that the driver's detects the dropped obstacle at about five seconds and immediately tries to avoid the obstacle by changing lane. The vehicle velocities at about five seconds of three cases, viz., NON-control, RI-based ROM, and RI/VS-based UCC, are similar to each other, as shown in Fig. 15(b).

When the UCC control is activated, two of the control systems yield good resistance to rollover, as shown in Fig. 15(c) and (e). As the RI-based ROM system intends to control the vehicle in a direction that is opposite to the driver's intention, the yaw rate

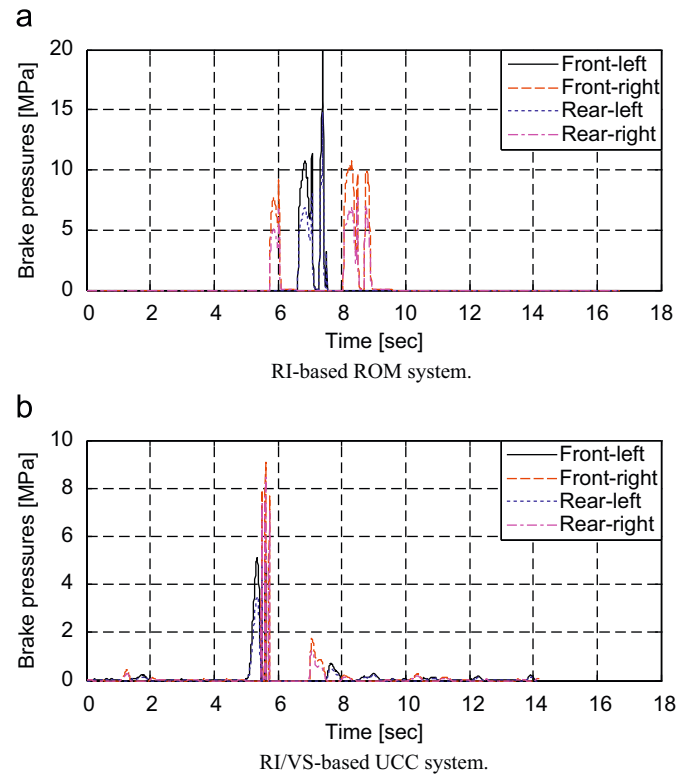


Fig. 16. Brake pressures.

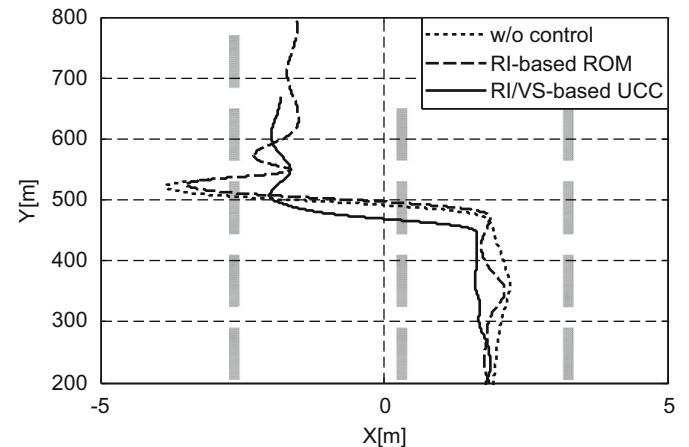


Fig. 17. Trajectories of the vehicle.

Table 2
Driving-test results of the 13 drivers.

Driver no.	Entrance speed (km/h)			Steering effort reduction (%)	Roll angle reduction (%)	Yaw rate error reduction (%)
	No control	RI-based	RI/Lat.-based			
1	94.4	94.8	95.1	33.5	40.7	67.3
2	93.7	99.5	100.5	44.9	26.7	56.2
3	93.8	96.5	96.2	15.4	13.4	29.2
4	100.4	102	102.8	63.9	32.6	61.5
5	99.1	96.4	99.7	32.9	26.6	31.8
6	94.5	100	100.1	61.3	16.3	48.2
7	98.9	100	100.6	37.8	25.0	47.9
8	101	99.1	100.2	40.2	26.9	41.0
9	94.4	94.8	94.4	50.0	47.9	62.2
10	97.8	97.2	98.5	54.4	27.2	53.9
11	97.4	100.7	100.6	36.7	55.9	56.2
12	94.5	98.5	100.7	45.4	48.0	46.9
13	94	99.9	101.3	41.7	37.9	23.1

error increases significantly at about 7 s, as shown in Fig. 15(f). At this point, the steering wheel angle also increases to compensate for the yaw rate error and to maintain the lane of travel, as shown in Fig. 15(a). It is observed that the yaw rate error and the steering wheel angle of the RI/VS-based UCC system are maintained at smaller values than under the RI-based ROM control system, as shown in Fig. 15(a) and (f). In the case of the RI/VS-based UCC system, the driver's steering effort for maintaining the lane is reduced by about 33.5% when compared with that under the RI-based ROM system. The roll angle and the yaw rate error are also reduced by about 40.7% and 67.3%, respectively.

Fig. 16 shows the brake pressures for two cases, namely RI-based ROM, and RI/VS-based UCC. In the case of the RI-based ROM system, the brake pressure increases because the controller intends to move the vehicle in a direction that is opposite to the driver's steering. Compared with the RI-based ROM case, only slight brake pressure is needed to prevent vehicle rollover while, at the same time, improving the maneuverability and lateral stability in the RI/VS-based UCC system.

The RI/VS-based UCC system shows the best tracking performance, as can be seen from Fig. 17. In the case of the RI-based ROM system, the vehicle deviates from the lane and secondary accidents may occur in spite of preventing vehicle rollover.

The test results of the thirteen drivers are analyzed and summarized in Table 2. The results of the proposed UCC system are compared with those of the previous RI-based ROM control scheme. Compared with the RI-based ROM control system, the proposed RI/VS-based UCC system reduces the driver's steering effort for maintaining the lane by up to about 63.9%. The roll angle and yaw rate error are reduced by up to about 55.9% and 67.3%, respectively.

5. Conclusion

This paper has described the evaluation of a rollover index (RI)/vehicle stability (VS)-based unified chassis control (UCC) algorithm by using a full-scale simulator on a virtual test track (VTT). The RI/VS-based UCC system has been proposed and compared with a prior RI-based ROM control system. A two-level control structure, i.e., with upper- and lower-level controllers, is adopted in this UCC system, which operates by switching across three control modes in the upper-level controller and switching across distribution schemes in the lower-level controller.

Real-time human-in-the-loop simulations have been conducted to verify the proposed RI/VS-based UCC control algorithm

through the driving simulator based on the VTT which is developed and used for the evaluation of the RI/VS-based UCC control system under various realistic conditions in a laboratory. One virtual driving test, an obstacle avoidance situation at high speed, is conducted to evaluate the performance of the rollover resistance and the vehicle stability aspects. In addition, the tests for thirteen drivers have also been conducted and the results analyzed. From these test results, it is verified that the proposed UCC system shows good performance for rollover prevention and improving the maneuverability and the lateral stability. Compared with the RI-based ROM system, it is shown that the proposed RI/VS-based UCC system reduces the driver's steering effort for maintaining the lane, and reducing roll angle and yaw rate error. In particular, from the viewpoint of maneuverability, the RI/VS-based UCC system is shown to be potentially superior to the RI-based ROM control system in terms of the yaw rate and the tracking error. This implies that the proposed RI/VS UCC system can prevent vehicle rollovers while, at the same time, improving the maneuverability of the vehicle.

For more accurate results, further evaluations under more varied conditions are required to substantiate the results presented. In addition, the proposed human-in-the-loop evaluation can be a good solution for determining of the dynamic threshold, which is required since an expert driver may feel redundant through frequent intervention of the control system, while the common vehicle stability control system is designed to be centered around the normal, average driver.

Acknowledgements

This work was supported by the MANDO Corporation, the BK21 program, SNU-IAMD, the Korea Research Foundation Grant funded by the Korean Government (MEST) (KRF-2009-200-D00003), and the National Research Foundation of Korea Grant funded by the Korean Government (2009-0083495).

References

- Chen, B. C., & Hsu, W. F. (2008). Sliding-mode control design of electric stability control for rollover prevention. *Proceedings of the AVEC 2008, Ninth international symposium on advanced vehicle control* (pp. 714–720).
- Chen, B. C., & Peng, H. (2001). Differential-braking-based rollover prevention for sport utility vehicles with human-in-the-loop evaluations. *Vehicle System Dynamics*, 36(4–5), 359–389.
- Cho, W., Yoon, J., & Yi, K. (2007). An investigation into unified chassis control scheme for optimized vehicle stability and maneuver-ability. *IAVSD 20th symposium* (pp. 242–263).

- Chung, T., & Yi, K. (2006). Design and evaluation of sideslip angle-based vehicle stability control scheme on a virtual test track. *IEEE Transactions on Control Systems Technology*, 14(2), 224–234.
- Hac, A., Brown, T., & Martens, J. (2004). Detection of vehicle rollover. *SAE Technical Paper*, 2004-01-1757
- Han, D., & Yi, K. (2006a). Evaluation of adaptive cruise control algorithms on a virtual test track. *Proceedings of the 2006 American control conference* (pp. 5849–5854).
- Han, D., & Yi, K. (2006b). Validation of a virtual test track for intelligent driver assistance system. *Proceedings of the AVEC 2006, Eighth international symposium on advanced vehicle control* (pp. 403–408).
- Han, D., Yi, K., & Yi, S. (2006). Evaluation of integrated ACC (adaptive cruise control)/CA (collision-avoidance) on a virtual test track. *ICE-ICASE international joint conference* (pp. 2127–2132).
- Jo, J., You, S., Joeng, J., Lee, K., & Yi, K. (2008). Vehicle stability control system for enhancing steerability, lateral stability, and roll stability. *International Journal of Automotive Technology*, 9(5), 571–579.
- Lee, H. (2004). Virtual test track. *IEEE Transactions on Vehicular Technology*, 53(6), 1818–8126.
- Nagai, M., Shino, M., & Gao, F. (2002). Study on integrated control of active front steer angle and direct yaw moment. *JSAE Review*, 23, 309–315.
- National Highway Traffic Safety Administration (NHTSA), F. (2003). *Motor vehicle traffic crash injury and fatality estimates, 2002 early assessment*. NCSA (National Center for Statistics and Analysis) Advanced Research and Analysis.
- National Highway Traffic Safety Administration (NHTSA), F. (2001). DOT Announces Proposal to Add Rollover Ratings to Auto Safety Consumer Information Program. *NHTSA Now*, 6(7).
- Park, J., Yoon, J., Yi, K., & Kim, D. (2008). Roll state estimator for rollover mitigation control. *Proceedings of the Institution of Mechanical Engineers (IMechE), Part D: Journal of Automobile Engineering*, 222, 1289–1311.
- Rajamani, R. (2006). *Vehicle dynamics and control*. New York: Springer (pp. 233–235).
- Schofield, B., & Hagglund, T. (2008). Optimal control allocation in vehicle dynamics control for rollover mitigation. *Proceedings of the 2008 American control conference* (pp. 3231–3236).
- Schubert, P. J., Nichols, D., Wallner, E. J., Kong, H., & Schiffmann, J. K. (2004). Electronics and algorithms for rollover sensing. *SAE Technical Paper*, 2004-01-0343
- Ungoren, A. Y., & Peng, H. (2004). Evaluation of vehicle dynamic control for rollover prevention. *International Journal of Automotive Technology*, 5(2), 115–122.
- Wielenga, T. J., & Chace, M. A. (2000). A study of rollover prevention using anti-rollover braking. *SAE Technical Paper*, 2000-01-1642
- Yang, H., & Liu, L. Y. (2003). A robust active suspension controller with rollover prevention. *SAE Technical Paper*, 2003-01-0959
- Yoon, J., Cho, W., Koo, B., & Yi, K. (2009). Unified chassis control for rollover prevention and lateral stability. *IEEE Transactions on Vehicular Technology*, 58(2), 596–609.
- Yoon, J., Kim, D., & Yi, K. (2007). Design of a rollover index-based vehicle stability control scheme. *Vehicle System Dynamics*, 45(5), 459–475.
- Yoon, J., Yi, K., Cho, W., & Kim, D. (2007). Unified chassis control to prevent vehicle rollover. *KSME spring conference* (pp. 895–900).
- You, S. H., Hahn, J. O., & Lee, H. (2009). New adaptive approaches to real-time estimation of vehicle sideslip angle. *Control Engineering Practice*, 17(12), 1367–1379.